Nanoscale

PAPER

View Article Online
View Journal | View Issue



Cite this: *Nanoscale*, 2016, **8**, 4984

# Fabrication and design of metal nano-accordion structures using atomic layer deposition and interference lithography†

J.-H. Min,[a] A. Bagal,[a] J. Z. Mundy,[b] C. J. Oldham,[b] B.-I. Wu,[c] G. N. Parsons[b] and C.-H. Chang*[a]

Received 2nd December 2015,
Accepted 2nd February 2016

DOI: 10.1039/c5nr08566g

www.rsc.org/nanoscale

Metal nanostructures have attractive electrical and thermal properties as well as structural stability, and are important for applications in flexible conductors. In this study, we have developed a method to fabricate and control novel complex platinum nanostructures with accordion-like profile using atomic layer deposition on lithographically patterned polymer templates. The template removal process results in unique structural transformation of the nanostructure profile, which has been studied and modeled. Using different template duty cycles and aspect ratios, we have demonstrated a wide variety of cross-sectional profiles from wavy geometry to pipe array patterns. These complex thin metal nanostructures can find applications in flexible/stretchable electronics, photonics and nanofluidics.

## 1. Introduction

In recent years there has been significant interest in flexible and stretchable electronics using nanoscale materials. One strategy to achieve mechanical compliance is to disperse zero-dimensional (0D), 1D, and 2D nanomaterials onto elastomeric substrates such as polydimenthylsiloxane (PDMS) or polymer-based materials.[1–3] In particular, nanomaterials with excellent electrical conductivity, such as nanoparticles,[4–6] carbon nanotubes,[7–9] and graphene,[10–14] have been widely studied. Another approach utilizes nanostructure geometry to increase flexibility of conducting materials.[15–17] Using wavy geometries caused by strain–release–buckling process, semiconducting or metallic structures can be stretched, compressed, and bent without property degradation. However, in this case the wavy geometries are typically in the microscale, and it is difficult to control precisely the buckle geometry.

One effective method to generate nanoscale films is atomic layer deposition (ALD), which can treat and functionalize surfaces of fabricated nanostructures and nanoscale devices with an ultra-thin material layer.[18–20] Using this benefit of ALD, many research groups have fabricated three-dimensional (3D) nanostructures including micro/nanolattice structures,[21–23] photonic crystals,[24] and nano-accordions.[25] In these processes, a broad range of materials (TiN, $Al_2O_3$, ZnO, *etc.*) were deposited onto sacrificial polymer templates, which are subsequently removed. The resulting final nanostructures consist of non-polymer material, and can have better physical properties when compared with the original polymer template. These advances have led to low-density materials with enhanced stiffness,[21–23] better photonic response,[24] and stretchable transparent conductors.[25]

For applications requiring better electrical and thermal conductivities and less brittleness, metal nanostructures can be an attractive solution. Various studies have shown ALD fabrication of thin conductive layer consisting of nickel,[26,27] tungsten,[28,29] or platinum[30–35] for electronics, solar cell components, and sensor devices, where the advantages of metal ALD including low resistivity, high purity, and excellent conformity can be specifically utilized. Others have also demonstrated freestanding metal nanostructures, including nickel nanotube,[36] ruthenium nanowire array,[37] and platinum nanobridge.[38] However, in existing studies the structures are mostly planar, relatively simple, and are difficult to control by the fabrication process.

Here we introduce a process to fabricate and control novel free-standing 3D metal nano-accordion structures using ALD and interference lithography (IL). In this approach, a lithographically defined periodic grating functions as a geometric template for conformal ALD coating of platinum (Pt). The polymer is subsequently removed using a thermal treatment process, leaving behind a free-standing metal structure with an

[a]*Department of Mechanical and Aerospace Engineering, North Carolina State University, Raleigh, North Carolina 27695, USA. E-mail: chichang@ncsu.edu*
[b]*Department of Chemical and Biomolecular Engineering, North Carolina State University, Raleigh, North Carolina 27695, USA*
[c]*Air Force Research Laboratory, Wright Patterson Air Force Base, OH 45433, USA*
†Electronic supplementary information (ESI) available. See DOI: 10.1039/c5nr08566g

accordion-like geometry. The profile of the final structure can take many forms and is determined by the polymer template and coating layer. The template feature height and width have dominant influence, and can be readily and systematically controlled by the lithography process. The complex nature of the structure profiles can potentially find applications in flexible/stretchable electronics, photonics, and nanofluidic devices.

## 2. Results and discussion

The proposed fabrication process is illustrated in Fig. 1, with corresponding scanning electron micrograph (SEM) images in the inset. Initially, 1D periodic photoresist structure were patterned using a Lloyd's mirror IL with 325 nm laser, as shown in Fig. 1(a).[39,40] The structure period, height, and feature width can be controlled by exposure angle, resist thickness, and exposure dose, respectively. The polymer structure was then deposited with a conformal Pt layer using ALD, which is the sole structure remaining after a subsequent thermal treatment process, as illustrated in Fig. 1(b) and (c), respectively. A negative-tone photoresist SU-8 was selected as the resist material due to its high glass transition temperature, since a relatively high process temperature is required for Pt ALD (for more information see ESI A†). A buffer layer of fully crosslinked SU-8 was used to improve adhesion template structure. After lithography, a hard bake at 210–220 °C was performed to fully crosslink the photoresist to improve material stability.

The cross-sectional SEM images in Fig. 1 illustrate the Pt nanostructure fabrication results after each processing steps. Here the period of SU-8 grating is 1 μm, and the width and height of the grating are 500 nm, achieving a duty cycle of 50% and an aspect ratio (AR) of 1. A thin alumina layer ($t \sim 2$ nm) was coated over the resist template to enhance surface reaction,[35,41] followed by 20 nm of Pt deposition, both using ALD. As shown in the SEM images of Fig. 1(b), the Pt grating structure on the resist template has high fidelity and good morphology throughout the whole sample with uniform thickness. After template removal process using convection oven at 550 °C, a free-standing metal nanostructure resembling an accordion remains on the silicon substrate, as shown in Fig. 1(c). The overall cross-sectional profile and period of the Pt structure has no significant changes, however the structure width was reduced by about 50%. In this case the SU-8 photoresist functions as a sacrificial template for fabricating and shaping the resulting thin nanostructured films. More information on the thermal and structural stability of Pt nanostructure is described in ESI A.†

X-ray photoelectron spectroscopy (XPS) measurement was performed to confirm the elemental composition of the thin Pt layer deposited by the ALD process, and is depicted in Fig. 2. A strong binding energy peak of ~71.0 eV can be observed, indicating that the film composition is pure metallic Pt.[33] An intermediate alumina layer between the resist and Pt layers was used in all samples to promote surface reaction, but it was not detected by XPS due to the limited thickness resolution. Without the alumina layer, direct Pt ALD on photoresist resulted in broadened energy peaks to indicate the presence of Pt oxides (for more information see ESI B†). Small peaks in the measurements indicate other elements such as oxygen and carbon, but are negligible.

To examine the electrical properties, the electrical properties of Pt nano-accordion structures were characterized by four-point probe system. The sheet resistances of the 20 nm-thickness Pt nanostructures on polymer template prior to the template removal process is 10.45 Ω per square, yielding a calculated film resistivity of 20.9 μΩ cm. After the template removal process to remove the underlying SU-8, the resistivity remained about the same and measured 20.7 μΩ cm. These data were measured with the probes parallel to the structure ridge direction. For comparison, the sheet resistance of planar 10 nm-thick Pt film on SU8 was measured to be 20.0 Ω per square, yielding comparable resistivity of 20.0 μΩ cm (for more data see ESI C†). These characterizations verify the material purity and metallic nature of the Pt nanostructure, as well as its uniformity of quality for different template geometries. The measured electrical conductivity of our Pt nano-accordion structure is comparable to that of the most recent works on stretchable electronics with existing conductive nanomaterials, such as metal nanowire,[42–45] carbon nanotube,[9,46–48] and graphene-based[13,49,50] electronics.

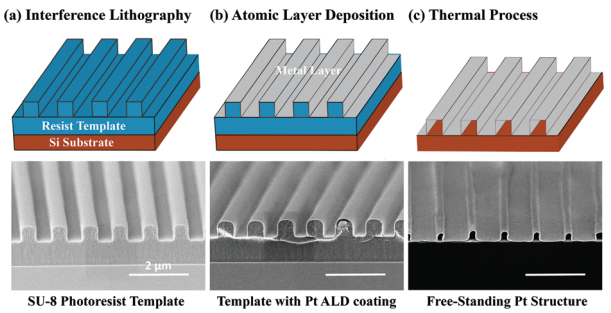


Fig. 1 Fabrication process and corresponding SEM images with scale bars of 2 μm. (a) Interference lithography on SU-8 photoresist to make a polymer grating template. (b) Platinum atomic layer deposition to coat the template surface with a conformal metal layer. (c) Thermal process to remove template, leaving behind a free-standing metal nano-accordion.

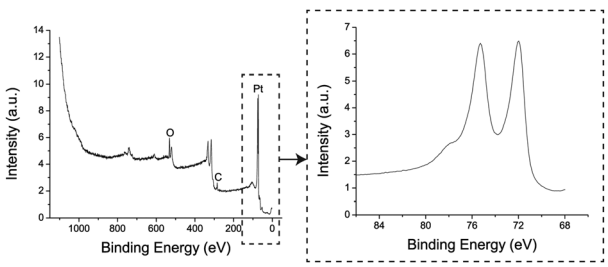


Fig. 2 Experimental XPS data of thin Pt structure deposited using ALD. A binding energy peak at 71.0 eV indicates pure metallic Pt.

Beyond material composition, the effects of resist template geometry on the final Pt nanostructure were also investigated. Two normalized geometric parameters, duty cycle (DC) = width/period and aspect ratio (AR) = height/width, were considered. The DC can be controlled by varying the energy dose. As observed in Fig. 1, the grating has rounded tops to resemble sinusoidal waves, but changes to flat tops to resemble square waves as the energy dose was increased to obtain a higher DC. In our experiments when the DC is higher than ~60%, the flat top grating was generated by IL and such a template structure induced a unique geometric deformation of the metal film during template removal after ALD.

The fabricated metal nanostructures can have complex profiles after the template removal process. Fig. 3(a) depicts a SEM image of the resist template with DC = 60% and AR = 0.83 before ALD. Significant changes in the resulting Pt structure profile were found after ALD and template removal processes, as shown in Fig. 3(b). In this case the grating failed to retain its original shape, unlike the case of round tops in Fig. 1. Fig. 3(c) shows a part of the sample after incomplete template removal under the Pt structure, caused by temperature gradient on polymer gratings. The structure deformation and collapse mechanisms can be identified by comparing each grating unit cell. The units on the left have more residual polymer and are observed to be less wrinkled compared to those on the right, offering a progression of the collapse process as polymers are removed. It can be observed that as the template is removed, the side walls and the ceiling collapse towards the center as the structure becomes wrinkled, creating a unique cross-sectional profile. Based on these results, the template geometry can be designed to control structure collapse and engineer the resulting Pt nanostructure.

In order to further study the profile formation process of the metal nano-accordions, we propose a first-order geometric model, as illustrated in Fig. 4(a). The key deformation mechanisms are the vertical sagging of the top ceiling and lateral collapse of the side walls associated with the template removal process, where the Pt films undergo structural wrinkling caused by the surface tension of evaporating SU-8. Based upon this mechanism, a uniform structure collapse rate ($v$) for the top and side walls of the grating unit is defined. As depicted in Phase I of Fig. 4(a), the structure starts to deform as the polymer template is being removed and the shape change occurs on both the top ceiling and the side walls. During the template removal process the wrinkling on ceiling and walls gets more pronounced (Phase II), finally resulting in the complex shape in Phase III, which was experimentally observed in Fig. 3(b). Based upon the proposed model, the structure profiles of Pt nano-accordions can be predicted by the grating width and height of the initial resist template, as illustrated in Fig. 4(b). In the case with AR < 1, the ceiling would collapse before sagging of side walls. When AR > 1, the two side walls merge before the ceiling collapses. In the intermediate regime where AR ~ 1, the ceiling and side walls are expected to collapse together. It is important to note that this model is restricted to flat-top template, and the wavy profile will not experience a significant geometric change for the round-top templates. In these cases, such as those shown in Fig. 1, the round curvature is more mechanically stable and is only expected to reduce in width, as illustrated in Fig. 4(c).

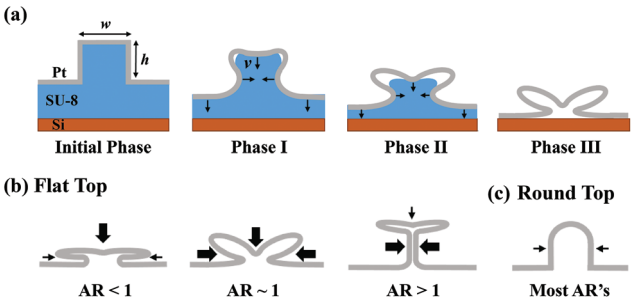


Fig. 4 Schematic of first-order geometric model for (a) flat-top Pt nano-accordion on polymer template during template removal process. (b) Predicted final profiles when AR is less than, around, and great than 1. (c) Predicted final profile for round-top Pt nano-accordions in most cases.

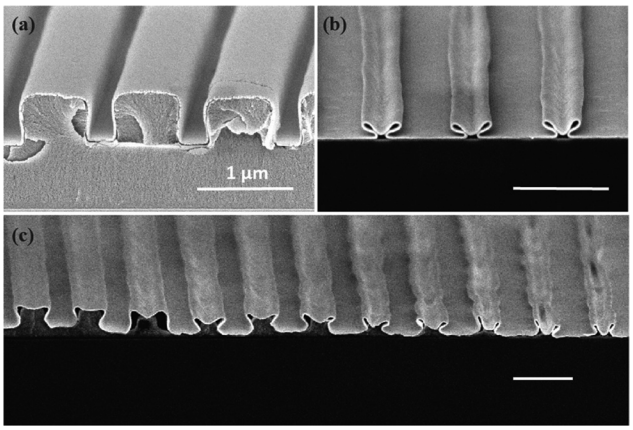


Fig. 3 SEM images (1 μm scale bars) of (a) Pt coating on resist template surface, and (b) Pt nano-accordion after template removal. (c) A region showing incomplete template removal and transition of structure deformation process.

To test the models for both flat-top and round-top templates, samples with height ranging from 300 nm to 1200 nm and width from 100 nm to 750 nm were fabricated, representing AR from 0.4 to 5.0. Fig. 5 shows comprehensive cross-sectional SEM images of the various metal nano-accordion profiles after template removal. The SEM images of the corresponding resist templates are shown in the inset diagrams. Two different top shapes were generated by controlling the duty cycle of the grating on the resist template. Flat-top templates in Fig. 5(a)–(c) were fabricated with DC = 60%, and round-tops in Fig. 5(d)–(f) were created with DC = 50%. The aspect ratios were controlled by varying the thickness of the resist template, exposure dose, or isotropic plasma etching (see ESI D†).

For flat-top templates, the AR was controlled by varying the resist thickness while fixing the template width. The general

 

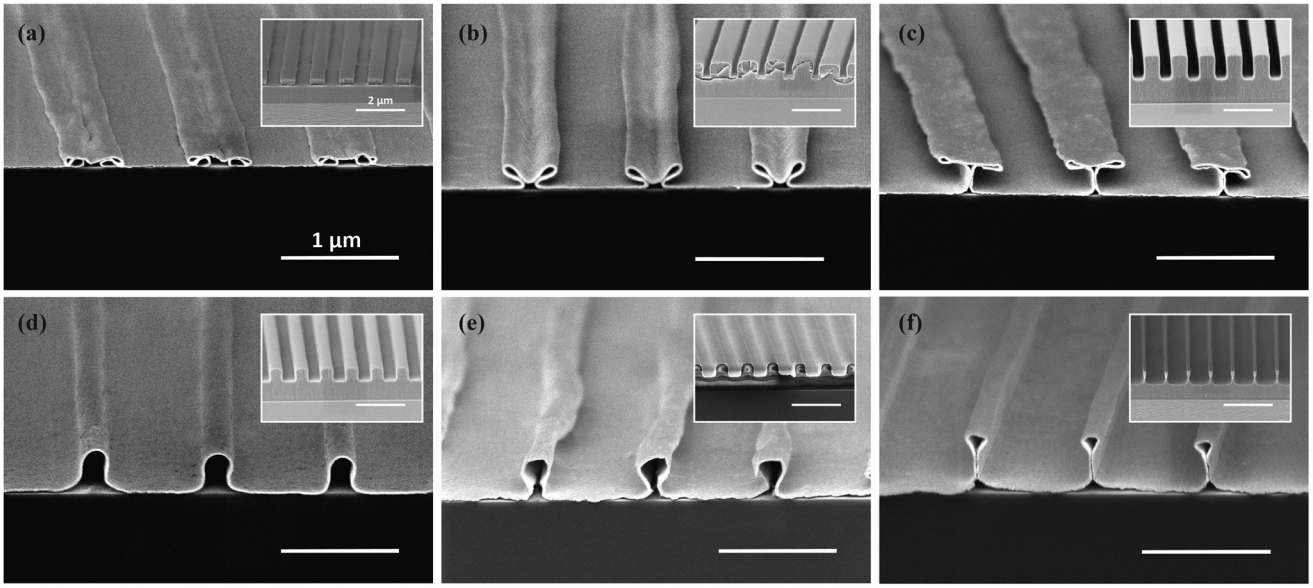


**Fig. 5** SEM images of free-standing Pt nano-accordion structures with (a)–(c) flat-top (DC = 60%) and (d)–(f) round-top templates (DC = 50%). The inset pictures in each image depict the photoresist template before thermal process. The structure aspect ratios (AR) are (a) 0.5, (b) 0.83, (c) 2.0, (d) 1.0, (e) 1.25, and (f) 5.0. Scale bars in main and inset images are 1 and 2 μm, respectively.

case of flat top is shown in Fig. 5(b), where the template used has an intermediate AR = 0.83. The final Pt structure resembles a sprout-like shape, indicating the ceiling sagging and side-wall collapses merged and terminated at around the same time. For the case of a template with lower AR = 0.5, as shown in Fig. 5(a), the ceiling completely collapsed prior to the wall and the final profile resemble mushroom-like shape. In the opposite extreme, a higher AR = 2 resulted in a T-like shape, as shown in Fig. 5(c), since the side wall collapses occurred prior to the ceiling. These results follow the general trend predicted by our geometric model described earlier.

For round-top templates, the fabricated cross-section profiles were less complex. In these samples oxygen plasma etching was used to control the template AR from 1 to 5, which preserves roundness without modifying the overall shape (for more information see ESI D†). After template removal, the top ceiling does not sag due to improved mechanical stability of the rounded ceiling and only the side walls collapse, in contrary to the flat-top templates. For low AR = 1, the resulting free-standing Pt structure closely resembles the original template profile, with about 50% decrease in structure width, as shown in Fig. 5(d). For template with AR = 1.25, the sidewall collapse developed further to result in a narrower waist, as shown in Fig. 5(e). For higher template AR = 5.0, the collapse of the sidewall was more pronounced, resulting in a sealed pipe-like shape, as shown in Fig. 5(f). The spaces enclosed by the Pt nanostructures are a distinguishable feature only observed on round top templates, and can potential find applications in nanofluidics.

The experimental results can be compared to the geometric model in a cross-section profile map defined by template width and height, as shown in Fig. 6. Lines of constant AR = 0.5, 1, and 2 are drawn to indicate the regimes of low, intermediate, and high AR, respectively. For low AR = 0.5, the final Pt structures are wrinkled and have completely collapsed. This represents the regime when the ceiling sagging is more dominant than the side wall collapse. This effect of immediate ceiling collapse is expected to be even more pronounced at AR < 0.5. For intermediate AR = 1. The ceiling sagging and wall collapse both play equally important roles, as the ceiling and side walls merge in the final structure to yield sprout-like profiles. On the other hand, for relatively high AR = 2, the side wall collapse is dominant and occurs prior to ceiling sagging. These structures generally have enclosed opening at the top of

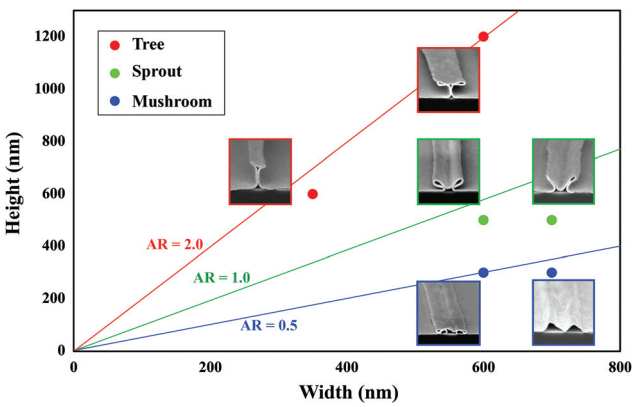


**Fig. 6** Cross-section profile map of fabricated Pt nano-accordion structures. The resulting structures are plotted as functions of template width and height. The ceiling sag is dominant when AR < 1, and the wall collapse is dominant when AR > 1. For AR ~ 1, both ceiling and wall collapses effects are equally important.

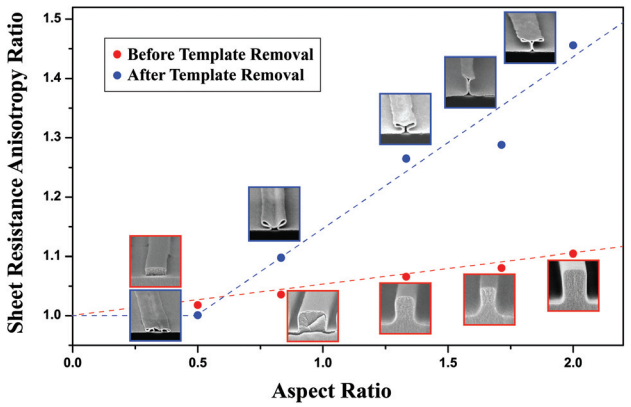


**Fig. 7** Sheet resistance anisotropy ratio ($R_{\perp}/R_{||}$) *vs.* aspect ratio for Pt nano-accordion structures before and after template removal. The ratio increases with increasing AR for both cases. The anisotropy is more significant after template removal with the resistance ratio up to 1.45, while it is limited to 1.10 for structures before template removal.

the structures while being sealed at the waist. The same effect is expected for AR greater than 2, where the sidewalls will collapse immediately and the ceiling will experience no geometrical change at all during the template removal process. Using this profile map, the final cross-sectional profiles of thin metal nanostructures can be predicted and designed for various applications.

Given the complex cross-sectional profile and high directionality of the Pt nanostructure, the anisotropy of electrical conductivity was further evaluated. Prior sheet resistances were measured parallel to the structure ridge direction ($R_{||}$). When the measurement probes are aligned in the perpendicular direction ($R_{\perp}$), the electrons follow the wavy profile in a more tortuous path and the structure could have higher resistance. The anisotropy ratio ($R_{\perp}/R_{||}$) of the fabricated Pt nano-accordions before and after template removal process are shown in Fig. 7 (for raw data see ESI E†). The anisotropy effect was small prior to template removal, gradually increasing with AR to yield a maximum of 10% increase for AR = 2. This can be attributed to sharper edges and roughness in higher AR structures.[51] However, the overall effect of AR was small since the structures do not have significantly different cross-sectional profile prior to template removal. The anisotropy ratio in free-standing Pt structures after template removal, on the other hand, has a stronger dependency on complexity of the structure. For low AR = 0.5 where structure has collapsed ceilings, anisotropy ratio is close to 1 to indicate no directional difference in sheet resistance. For the sprout-like profile structure with AR = 0.83, the complex geometry resulted in $R_{\perp}$ being about 10% higher than $R_{||}$. At even higher AR = 2, the anisotropy increased to more than 45% due to more complicated profiles and sharper edges. Complex profiles also lead to more structure collapse during the template removal process, which can result in crack formation along the structure ridge direction and increase anisotropic effects. These characterizations demonstrates that Pt nanostructures with complex cross-sectional profiles can maintain high conductivity in along orthogonal directions parallel and perpendicular to the fold geometry. These structures can potentially be transferred to flexible substrates for stretchable devices, and the dependence of electrical properties on strain is the subject of future studies.

## 3. Conclusions

In this work we have demonstrated Pt nano-accordion structures with complex cross-sectional profiles using a combination of ALD and IL. These metal nanostructures have good structural stability and electrical conductivity, and their cross-sectional profiles can be designed by specifying the template geometry. Pt structures undergo structural transformation during the template removal process, which can be qualitatively predicted using the proposed geometric model base on structure duty cycle and aspect ratio. This model generates a cross-section profile map, where the structure geometry can be designed as functions of template width and height. These free-standing nanostructures exhibit anisotropic electrical properties, with sheet resistance up to 45% higher in the direction perpendicular to the structure ridge for the most complex profile. These structures can also potentially be stretched, leading to future applications in stretchable electronic and photonic devices.

## 4. Experimental section

For fabrication of photoresist template, 90 nm thick anti-reflection coating (ARC i-CON-7, Brewer Science, Inc.) and 500 nm of SU-8 (Microchem, Corp.) were spin-coated on a silicon wafer to prevent back-reflection during lithography and create a buffer layer, respectively. SU-8 was spin-coated on top of the buffer layer and soft-baked at 95 °C. An interference lithography setup with HeCd laser (wavelength of 325 nm) was used to pattern the template grating with 1 μm period. A range of exposure dose from 3–6 mJ $cm^{-2}$ was used to control the template feature width. After exposing process, the samples were post-expose-baked at 65 °C, developed with propylene glycol monomethyl ether acetate (PGMEA), and rinsed in Isopropyl Alcohol (IPA) followed by hard-bake at 220 °C.

An intermediate $Al_2O_3$ layer was coated on the polymer template using ALD in a custom-built vacuum reactor (1 Torr at 200 °C). A metal precursor, trimethylaluminum (TMA, 98% pure, Strem Chemicals) is first dosed for 0.5 seconds, followed by nitrogen (filter-dried by Entegris GateKeeper, 99.999% pure) purge for 30 seconds, and then a co-reactant, UV-deionized water, is dosed into the chamber for 0.5 seconds, followed by another nitrogen purge for 30 seconds. The growth rate is about 1.3 Å per cycle, and 15 cycles were conducted to deposit around 2 nm of $Al_2O_3$. A platinum was then coated on the intermediate alumina layer (1 Torr at 200 °C) using (methylcyclopentadienyl)trimethylplatinum ($MeCpPtMe_3$) as

 

the precursor and ozone as the reactant gas.[33–35] The typical dosing scheme is composed of 4 second for Pt precursor dose, 5 seconds of Pt precursor hold, 30 seconds of nitrogen purge, and then 4 second for ozone dose, 5 seconds of ozone hold, 30 seconds of nitrogen purging. The hold steps were included to effectively increase precursor and reactant exposure to the target substrate. The Pt precursor, $MeCpPtMe_3$ (99% pure, Strem Chemicals) was prepared at 60 °C in a stainless steel vessel and the ozone was generated from research-grade oxygen (99.999% pure, Machine & Welding Supply Company) with concentration set to 11 wt%. The platinum growth rate is about 0.45 Å per cycle, and 420 cycles were repeated to deposit around 20 nm of metallic Pt for most samples.

Finally, the template removal process was performed using convection oven at 550 °C. Slow temperature ramping of 0.5–1.0 °C per minute was used to avoid structure collapse attributed to sudden temperature changes. The samples were then treated with oxygen plasma to clean organic contaminants and other residuals.

## Acknowledgements

We gratefully acknowledge the students, staff, and facility support from the North Carolina State University Nanofabrication Facility (NNF). The authors also acknowledge the use of the Analytical Instrumentation Facility (AIF) at North Carolina State University, which is supported by the State of North Carolina and the National Science Foundation. This work was supported by a NASA Office of the Chief Technologist's Space Technology Research Opportunity – Early Career Faculty grant (grant NNX12AQ46G) and Air Force Research Laboratory.

## References

1 J. A. Rogers, T. Someya and Y. Huang, *Science*, 2010, **327**, 1603–1607.
2 S. Yao and Y. Zhu, *Adv. Mater.*, 2015, **27**, 1480–1511.
3 J.-H. Ahn and J. H. Je, *J. Phys. D: Appl. Phys.*, 2012, **45**, 103001.
4 D. C. Hyun, M. Park, C. Park, B. Kim, Y. Xia, J. H. Hur, J. M. Kim, J. J. Park and U. Jeong, *Adv. Mater.*, 2011, **23**, 2946–2950.
5 Y. Kim, J. Zhu, B. Yeom, M. Di Prima, X. Su, J.-G. Kim, S. J. Yoo, C. Uher and N. a. Kotov, *Nature*, 2013, **500**, 59–63.
6 M. Park, J. Im, M. Shin, Y. Min, J. Park, H. Cho, S. Park, M.-B. Shim, S. Jeon, D.-Y. Chung, J. Bae, J. Park, U. Jeong and K. Kim, *Nat. Nanotechnol.*, 2012, **7**, 803–809.
7 T. Yamada, Y. Hayamizu, Y. Yamamoto, Y. Yomogida, A. Izadi-Najafabadi, D. N. Futaba and K. Hata, *Nat. Nanotechnol.*, 2011, **6**, 296–301.
8 D. J. Lipomi, M. Vosgueritchian, B. C.-K. Tee, S. L. Hellstrom, J. A. Lee, C. H. Fox and Z. Bao, *Nat. Nanotechnol.*, 2011, **6**, 788–792.
9 K.-Y. Chun, Y. Oh, J. Rho, J.-H. Ahn, Y.-J. Kim, H. R. Choi and S. Baik, *Nat. Nanotechnol.*, 2010, **5**, 853–857.
10 R. H. Kim, M. H. Bae, D. G. Kim, H. Cheng, B. H. Kim, D. H. Kim, M. Li, J. Wu, F. Du, H. S. Kim, S. Kim, D. Estrada, S. W. Hong, Y. Huang, E. Pop and J. a. Rogers, *Nano Lett.*, 2011, **11**, 3881–3886.
11 K.-Y. Shin, J.-Y. Hong and J. Jang, *Chem. Commun.*, 2011, **47**, 8527–8529.
12 X. Li, Y. Zhu, W. Cai, M. Borysiak, B. Han, D. Chen, R. D. Piner, L. Colombo and R. S. Ruoff, *Nano Lett.*, 2009, **9**, 4359–4363.
13 K. S. Kim, Y. Zhao, H. Jang, S. Y. Lee, J. M. Kim, K. S. Kim, J.-H. Ahn, P. Kim, J.-Y. Choi and B. H. Hong, *Nature*, 2009, **457**, 706–710.
14 Z. Chen, W. Ren, L. Gao, B. Liu, S. Pei and H.-M. Cheng, *Nat. Mater.*, 2011, **10**, 424–428.
15 D.-H. Kim, N. Lu, R. Ma, Y.-S. Kim, R.-H. Kim, S. Wang, J. Wu, S. M. Won, H. Tao, A. Islam, K. J. Yu, T. Kim, R. Chowdhury, M. Ying, L. Xu, M. Li, H.-J. Chung, H. Keum, M. McCormick, P. Liu, Y.-W. Zhang, F. G. Omenetto, Y. Huang, T. Coleman and J. A. Rogers, *Science*, 2011, **333**, 838–843.
16 S. Yao and Y. Zhu, *Nanoscale*, 2014, **6**, 2345–2352.
17 S. Xu, Z. Yan, K. Jang, W. Huang, H. Fu, J. Kim, Z. Wei, M. Flavin, J. Mccracken, R. Wang, A. Badea, Y. Liu, D. Xiao, G. Zhou, J. Lee, H. U. Chung, H. Cheng, W. Ren, A. Banks, X. Li, U. Paik, R. G. Nuzzo, Y. Huang and J. A. Rogers, *Science*, 2015, **347**, 154–157.
18 M. Knez, K. Nielsch and L. Niinistö, *Adv. Mater.*, 2007, **19**, 3425–3438.
19 H. Kim, H. B. R. Lee and W. J. Maeng, *Thin Solid Films*, 2009, **517**, 2563–2580.
20 S. M. George, *Chem. Rev.*, 2010, **110**, 111–131.
21 D. Jang, L. R. Meza, F. Greer and J. R. Greer, *Nat. Mater.*, 2013, **12**, 893–898.
22 C. Bae, H. Shin and K. Nielsch, *MRS Bull.*, 2011, **36**, 887–897.
23 X. Zheng, H. Lee, T. H. Weisgraber, M. Shusteff, J. DeOtte, E. B. Duoss, J. D. Kuntz, M. M. Biener, Q. Ge, J. a. Jackson, S. O. Kucheyev, N. X. Fang and C. M. Spadaccini, *Science*, 2014, **344**, 1373–1377.
24 S.-G. Park, T. Y. Jeon, H. C. Jeon, S.-M. Yang, J.-D. Kwon, C.-W. Mun, B. Cho, C. S. Kim and D.-H. Kim, *J. Mater. Chem. C*, 2014, **2**, 1957–1961.
25 A. Bagal, E. C. Dandley, J. Zhao, X. a. Zhang, C. J. Oldham, G. N. Parsons and C.-H. Chang, *Mater. Horiz.*, 2015, **2**, 486–494.
26 M. Utriainen, M. Kröger-Laukkanen, L. S. Johansson and L. Niinistö, *Appl. Surf. Sci.*, 2000, **157**, 151–158.
27 J. Chae, H.-S. Park and S. Kang, *Electrochem. Solid-State Lett.*, 2002, **5**, C64–C66.
28 J. W. Klaus, S. J. Ferro and S. M. George, *Thin Solid Films*, 2000, **360**, 145–153.
29 B. Kalanyan, C. J. Oldham, W. J. Sweet and G. N. Parsons, *ACS Appl. Mater. Interfaces*, 2013, **5**, 5253–5259.

30 T. Aaltonen, M. Ritala, T. Sajavaara, J. Keinonen and M. Leskelä, *Chem. Mater.*, 2003, **15**, 1924–1928.
31 T. Aaltonen, M. Ritala, Y.-L. Tung, Y. Chi, K. Arstila, K. Meinander and M. Leskelä, *J. Mater. Res.*, 2004, **19**, 3353–3358.
32 A. J. M. MacKus, D. Garcia-Alonso, H. C. M. Knoops, A. a. Bol and W. M. M. Kessels, *Chem. Mater.*, 2013, **25**, 1769–1774.
33 J. Dendooven, R. K. Ramachandran, K. Devloo-Casier, G. Rampelberg, M. Filez, H. Poelman, G. B. Marin, E. Fonda and C. Detavernier, *J. Phys. Chem. C*, 2013, **117**, 20557–20561.
34 H. B. R. Lee, K. L. Pickrahn and S. F. Bent, *J. Phys. Chem. C*, 2014, **118**, 12325–12332.
35 J. Z. Mundy, A. Shafiefarhood, F. Li, S. A. Khan and G. N. Parsons, *J. Vac. Sci. Technol., A*, 2016, **34**, 01A152.
36 M. Daub, M. Knez, U. Goesele and K. Nielsch, *J. Appl. Phys.*, 2007, **101**, 09J111.
37 W.-H. Kim, S.-J. Park, J.-Y. Son and H. Kim, *Nanotechnology*, 2008, **19**, 045302.
38 S. Yoneoka, J. Lee, M. Liger, G. Yama, T. Kodama, M. Gunji, J. Provine, R. T. Howe, K. E. Goodson and T. W. Kenny, *Nano Lett.*, 2012, **12**, 683–686.
39 H. I. Smith, *Physica E*, 2001, **11**, 104–109.
40 A. Bagal and C.-H. Chang, *Opt. Lett.*, 2013, **38**, 2531–2534.
41 G. N. Parsons, S. E. Atanasov, E. C. Dandley, C. K. Devine, B. Gong, J. S. Jur, K. Lee, C. J. Oldham, Q. Peng, J. C. Spagnola and P. S. Williams, *Coord. Chem. Rev.*, 2013, **257**, 3323–3331.
42 F. Xu and Y. Zhu, *Adv. Mater.*, 2012, **24**, 5117–5122.
43 P. Lee, J. Lee, H. Lee, J. Yeo, S. Hong, K. H. Nam, D. Lee, S. S. Lee and S. H. Ko, *Adv. Mater.*, 2012, **24**, 3326–3332.
44 W. Hu, X. Niu, L. Li, S. Yun, Z. Yu and Q. Pei, *Nanotechnology*, 2012, **23**, 344002.
45 J. Liang, L. Li, K. Tong, Z. Ren, W. Hu, X. Niu, Y. Chen and Q. Pei, *ACS Nano*, 2014, **8**, 1590–1600.
46 T. Sekitani, Y. Noguchi, K. Hata, T. Fukushima, T. Aida and T. Someya, *Science*, 2008, **321**, 1468–1472.
47 T. Sekitani, H. Nakajima, H. Maeda, T. Fukushima, T. Aida, K. Hata and T. Someya, *Nat. Mater.*, 2009, **8**, 494–499.
48 L. Hu, W. Yuan, P. Brochu, G. Gruner and Q. Pei, *Appl. Phys. Lett.*, 2009, **94**, 161108.
49 S. Bae, H. Kim, Y. Lee, X. Xu, J.-S. Park, Y. Zheng, J. Balakrishnan, T. Lei, H. Ri Kim, Y. Il Song, Y.-J. Kim, K. S. Kim, B. Özyilmaz, J.-H. Ahn, B. H. Hong and S. Iijima, *Nat. Nanotechnol.*, 2010, **5**, 574–578.
50 M. Lee, K. Lee, S. Kim, H. Lee, J. Park, K. Choi, H. Kim, D. Kim, D. Lee, S. Nam and J. Park, *Nano Lett.*, 2013, **13**, 2814–2821.
51 H. Marom and M. Eizenberg, *J. Appl. Phys.*, 2006, **99**, 123705.

 